Remote Sensing of Environment 115 (2011) 2674–2685

Contents lists available at ScienceDirect

Remote Sensing of Environment

journal homepage: www.elsevier.com/locate/rse

Algorithm for retrieval of the effective snow grain size and pollution amount from satellite measurements

E.P. Zege [a], I.L. Katsev [a], A.V. Malinka [a,*], A.S. Prikhach [a], G. Heygster [b], H. Wiebe [b]

[a] B.I. Stepanov Institute of Physics, National Academy of Sciences of Belarus, 220072, Pr. Nezavisimosti 68, Minsk, Belarus
[b] Institute of Environmental Physics, University of Bremen, Bremen, Germany O. Hahn Allee 1, D-28359 Bremen, Germany

ARTICLE INFO

Article history:
Received 13 July 2010
Received in revised form 2 June 2011
Accepted 2 June 2011
Available online 12 July 2011

Keywords:
Satellite
Remote sensing
Snow
Pollution

ABSTRACT

We present an algorithm for retrieval of the effective Snow Grain Size and Pollution amount (SGSP) from satellite measurements. As well as our previous version (Zege et al., 2008, 1998), the new algorithm is based on the analytical solution for snow reflectance within the asymptotic radiative transfer theory. The SGSP algorithm does not use any assumptions on snow grain shape and allows for the snow pack bidirectional reflectance distribution function (BRDF). The algorithm includes a new atmospheric correction procedure that allows for snow BRDF. This SGSP algorithm has been thoroughly validated with computer simulations. Its sensitivity to the atmosphere model has been investigated. It is shown that the inaccuracy of the snow characteristic retrieval due to the uncertainty in the aerosol and molecular atmosphere model is negligible, as compared to that due to the measurement errors at least for aerosol loads typical for polar regions. The significant advantage of the SGSP over conventional algorithms, which use a priori assumptions about particle shape and (or) not allow for the BRDF of the individual snow pack, is that the developed retrieval still works at low sun elevations, which are typical for polar regions.

1. Introduction

Snow affects the local and global radiative balances of the Earth. The polar caps, covered with a snow blanket all-the-year-round, play a key role in the Earth radiation budget. The pollution of snow, e.g., from industrial sources, drastically affects the snow radiation regime and ice melting. The extent of snow covered area, as well as the snow albedo, r, can influence the Earth's climate. The two main parameters, which define the radiative properties of snow, are the grain size and the pollution amount.

Satellite remote sensing is an important tool for snow cover monitoring, especially over difficult-to-access polar regions. The core of the remote sensing algorithms is the relation between measured radiative and retrieved microphysics characteristics.

The classical works on snow remote sensing (Bohren, 1974; Wiscombe & Warren, 1980a,b) consider snow as a layer consisting of large spherical particles. From the very beginning the satellite algorithms to retrieve the snow effective grain size from the measured spectral reflection characteristics employ this snow model (Grenfell et al., 1994; Li et al., 2001; Hori et al., 2001). They use Mie scattering theory to compute the snow inherent optical properties and the radiative transfer codes to develop look-up-tables (LUT) that are used for the inversion procedure.

However, as it follows from numerous experimental studies of microphysics snow properties (Aoki et al., 2000, 2003; Massom et al., 2001; Matzl & Schneebeli, 2006; Kerbrat et al., 2008), the snow grain shapes are far from ideal spheres and vary, depending on the origin and the age of snow and on the environmental conditions. Therefore, a snow pack should be considered as a multiple scattering close packed medium with irregularly shaped grains. Note that the shapes of snow grains are not known a priori. Such a model was suggested by Zege et al. (1998). The idea of an algorithm to retrieve the snow grain size and pollution amount, based on this snow model with no a priori assumptions on snow grain shapes, was put forward by the authors in the process of a pre-launch investigation for the GLI aboard ADEOS and shortly published in Zege et al. (1998). This algorithm was completely analytical; it used the analytical asymptotic solution for the radiative transfer equation developed in Zege et al. (1991) and geometrical optics for single-scattering characteristics, described afterwards in Kokhanovsky and Zege (2004). Later this idea was used in the algorithm SGSP (Snow Grain Size and Pollution) as applied to the MODIS instrument (Zege et al., 2008). Since that time a few new algorithms to retrieve snow grain size and pollution amount that are based on the proposed approach were developed (Tedesco & Kokhanovsky, 2007; Lyapustin et al., 2009).

Still the algorithm (Zege et al., 2008) differs from all others in one important feature: it does not use any a priori assumption of the snow BRDF. As it is shown in this paper this feature is of a great importance, particularly for polar regions with the low sun. Nevertheless, the algorithm (Zege et al., 2008) lacked a reliable and verified procedure

* Corresponding author. Tel.: +375 17 2841997.
E-mail addresses: eleonor@light.basnet.by (E.P. Zege), mal@light.basnet.by (A.V. Malinka).

0034-4257/$ – see front matter © 2011 Elsevier Inc. All rights reserved.
doi:10.1016/j.rse.2011.06.001

of the atmospheric correction. In this paper we present the mature algorithm to retrieve the snow grain size and pollution amount with verified atmosphere correction procedure that meets accuracy requirement for monitoring polar regions with low sun positions. This algorithm currently is implemented for MODIS instrument.

The SGSP code runs through a Windows graphic user interface and as a Linux console application. Currently, the presented version of the SGSP code with the atmospheric correction procedure, arranged as a Linux console application, routinely works in the MODIS processing chain in Bremen University, providing MODIS snow product for selected polar regions. The daily maps and the online archive can be found at http://www.iup.uni-bremen.de:8084/amsr/modis.html. The maps of the previous days can be found in the online archive http://www.iup.uni-bremen.de:8084/amsredata/modis/.

This paper is arranged as follows. Radiative characteristics of a snow pack on the base of our works (Zege et al., 1998, 2008) are overviewed in Section 2. Practically Section 2 is completely based on these published earlier results of the authors and briefly sums them to introduce values and relations that are necessary for understanding what follows. In Section 3 we discuss the different currently used approximations for the angular radiance distribution at the top of the atmosphere–snow system and show that their accuracy does not meet the requirements of the inverse problem. We offer a more accurate approach in regard to the real snow BRDF. Section 4 introduces the developed Windows tool, the SRS (Snow Reflection Simulator) software. SRS simulates the bi-directional reflectance of a snow–atmosphere system and the signals in the spectral channels of satellite optical instruments. Computer verification of the approach proposed in Section 3 for the radiance at the top of the atmosphere–snow system with accent to polar regions is presented in Section 5. The final version of the SGSP algorithm with an iterative atmospheric correction procedure is presented in Section 6. Section 7 discusses the flow-chart of the SGSP algorithm. Then, in Section 8 the verification of the SGSP algorithm is presented and discussed. Conclusion sums up this paper.

2. Radiative characteristics of thick snow layer

As it was shown in Zege and Kokhanovsky (1997); Zege et al. (1998); Kokhanovsky and Zege (2004) using the asymptotic solution of the radiative transfer theory, the spherical albedo r (bi-hemispherical reflectance) of a semi-infinite layer and its plane albedo $r(\theta_0)$ (hemispherical reflectance at incidence with zenith angle θ_0) can be calculated as:

$$r = \exp(-y), \qquad r(\theta_0) = \exp(-y\,g(\theta_0)), \tag{1}$$

where

$$g(\theta_0) = \frac{3}{7}(1 + 2\cos\theta_0), \qquad y = 4\sqrt{\frac{\sigma_a}{3\sigma_e(1-g)}}. \tag{2}$$

Here σ_e and σ_a are the extinction and absorption coefficients, respectively, g is the average cosine of the phase function of the medium.

When considering snow as a layer of non-spherical close-packed grains of different shapes, in the framework of geometrical optics (Zege et al., 1998; Kokhanovsky & Zege, 2004), the aforementioned characteristics of pure snow in visible and near IR are:

$$\sigma_e = \frac{1.5\,C_V}{a_{ef}}, \quad \sigma_a = \xi\frac{4\pi\chi}{\lambda}C_V. \tag{3}$$

Here C_V is the volumetric snow particle concentration, a_{ef} is the effective grain size, equal to the radius of the volume-to-surface equivalent sphere:

$$a_{ef} = \frac{3\langle V\rangle}{4\langle\Sigma\rangle}, \tag{4}$$

where $\langle V\rangle$ and $\langle\Sigma\rangle$ are the average volume and the average cross-section (geometric shadow) area of the snow grains, respectively; χ is the imaginary part of the complex refractive index of ice, λ is the wavelength, ξ is a factor that depends on the particle shape.

Substituting Eq. (3) into Eq. (2), we get:

$$y = A\sqrt{\frac{4\pi\chi}{\lambda}a_{ef}}, \tag{5}$$

where

$$A = \frac{4}{3}\sqrt{\frac{2\xi}{1-g}}, \tag{6}$$

the factor that depends on the particle shape only.

Some computations of the values of A for non-spherical particles are given by Kokhanovsky and Macke (1997), where they got for fractal particles the value of $A = 5.1$. Some more values for various grain shapes are proposed in Picard et al. (2009). Pay attention, that in these works (and in many others on snow remote sensing), authors define the effective size as a diameter of a sphere with equivalent volume-to-surface ratio, while we (keeping tradition of optics of scattering media) define it as a radius, see Eq. (4). It is why in the cited papers factor A, by definition, differs by the square of two. The values of A for a mixture of hexagonal ice columns and plates, obtained with code by Yang and Liou (1996) (Geometric-optics-integral-equation method) with surface roughness model improved by Shcherbakov et al. (2006), are given in Table 1.

Hereafter, we will consider the fifty–fifty mixture of chaotically oriented ice hexagonal plates (with aspect ratio of 1/4) and columns (with aspect ratio 4/1) with rough surfaces. This model will be referred to as the MIX model in what follows. Note that preliminary computations with the code by Yang and Liou (1996) showed that the optical properties of the mixture of the large ice crystals with rough surfaces do not vary considerably with changes of the aspect ratios of ice hexagons in a mixture. Although we will often use the MIX model throughout the paper and compare it to the model of spheres, we do not pretend that it is a representative model for real snow microstructure. We would just like to use a model of snow grains that are far from spheres to demonstrate that our algorithm allows one to retrieve the grain effective size regardless of their shape. The traditional approaches, based on particular shape models, may give extremely incorrect values if the a priori shape model is chosen wrong. In the approach we are presenting the only parameter that depends on the grain shape is parameter A. The calculations performed with a Mie code show that for spheres this parameter is approximately 6.5. So, A ranges approximately from 5.1 for fractals to 6.5 for spheres. It means that the error of the snow grain size retrieval from snow radiation characteristics due to the uncertainty of the value of parameter A is not larger than 25%. In our calculations we use the average value of 5.8 for parameter A and value of 1.5 for factor ξ,

Table 1
Computations of the form-factor A for the MIX model of snow grains.

Grain size / Wavelength	30 μm	100 μm	300 μm
870 nm	6.05	5.76	5.50
1240 nm	5.97	5.81	5.75

with no regard to the predefined grain shape. Obviously, the value of these parameters could be adjusted, according to experimental data on real snow. Unfortunately, by the moment we do not have enough experimental data to make a conclusion. We should emphasize, however, that the uncertainty in knowledge of parameter A, although it produces the uncertainty in the retrieved grain size, does not affect the reflection characteristics of a snow pack, such as spectral albedo, e.g., because the radiative characteristics of a layer depend again on product $A^2 a_{eff}$.

Let us consider now the soot pollution of snow. Soot particles are very fine with radius smaller than 0.1 μm. The refractive index of soot is $m_{st} = n_{st} - i\chi_{st} = 1.75 - 0.43i$ (Lenoble, 1986) in the visible and near IR spectra. Light scattering by such particles is extremely small in comparison to scattering by snow grains. Thus, the effect of soot impurities on the light scattering in snow can be ignored.

The absorption coefficient of soot particles is equal to (Bohren & Huffman, 1983):

$$\sigma_a^{st} = \frac{3Q_a^{st}}{4r_{ef}^{st}} C_{st}, \tag{7}$$

where Q_a^{st} is the soot absorption efficiency, r_{ef}^{st} is the effective radius of soot particles, C_{st} is the soot volumetric concentration. In what follows the amount of the soot pollution will be characterized by the relative soot concentration $C_{st}^* = C_{st}/C_V$, where C_{st} and C_V are the soot and snow grain volumetric concentrations, respectively. They relate to the commonly used mass concentrations as:

$$C_i = M_i / \rho_i, \quad i = soot, ice, \tag{8}$$

where ρ_i is the substance (soot or ice) mass density, and M_i is the mass concentration of particles. Then the absorption coefficient of polluted snow at wavelength λ is characterized by:

$$\sigma_a = \sigma_a^{snow} + \sigma_a^{st} = \frac{4\pi}{\lambda} \xi C_V (\chi + kC_{st}^*), \tag{9}$$

where

$$k = \frac{3Q_a^{st}\lambda}{16\pi r_{ef}^{st}\xi}. \tag{10}$$

The computations by Mie theory according to the *Soot* model (Lenoble, 1986) show that in the range of interest $k \simeq 0.2$.

The value of y (Eq. (2)) through Eqs. (3) and (9) therefore becomes:

$$y = A\sqrt{\frac{4\pi}{\lambda} a_{ef}(\chi + kC_{st}^*)} = Aq\sqrt{a_{ef}}, \tag{11}$$

where

$$q = \sqrt{4\pi \frac{\chi + kC_{st}^*}{\lambda}} \tag{12}$$

is the only value in Eq. (11) that depends on wavelength.

The BRDF of the semi-infinite snow layer $R(\theta, \theta_0, \varphi)$ can be calculated from the asymptotic theory of radiation transfer (Zege et al., 1991):

$$R(\theta, \theta_0, \varphi) = R_0(\theta, \theta_0, \varphi)\ exp\left[-y \frac{g(\theta)g(\theta_0)}{R_0(\theta, \theta_0, \varphi)}\right], \tag{13}$$

where θ and θ_0 are polar (zenith) angles of the observation and the sun, respectively (here and throughout the paper these angles are counted from the zenith), φ is the azimuth angle; $R_0(\theta, \theta_0, \varphi)$ is the BRDF of the semi-infinite non-absorbing layer with the same scattering phase function.

The BRDF of the semi-infinite non-absorbing layer $R_0(\theta, \theta_0, \varphi)$ depends on the phase function of the medium only. However, this dependence is quite strong due to notable contribution of single scattering, especially at the oblique incidence. The phase function in its turn depends strongly on the particle shape. In the framework of geometrical optics, when the particles are much larger than the wavelength, the phase function is completely defined by the particle shape and the real part of the refractive index. As the real part of the ice refractive index has a weak spectral dependence in the visible and near IR, the spectral changes of the phase function, and consequently, of function $R_0(\theta, \theta_0, \varphi)$, are negligible.

In Fig. 1 the phase functions for the MIX and spherical particles models at wavelengths 469 nm, 858.5 nm, and 1240 nm are plotted (these wavelengths correspond to MODIS channels 3, 2, and 5). The Yang code (Yang & Liou, 1996) was used in calculations for the MIX model and the Mie code for the model of spherical particles. It is seen that the phase functions of spheres at different wavelengths differ only in the range near the rainbow angle (~40°) and there is practically no spectral difference for the MIX model. However, these phase functions differ a lot for different grain shape models. The greatest difference (more than ten times) is localized near the scattering angle of 100°. This minimum of the phase function in the range of 90°–120° is the inherent feature of spherical particles. This range of scattering angles is typical for satellite observation in polar regions, where the sun incidence is oblique. That is why the common way of satellite snow grains sizing based on Mie computations gives unreliable results in polar regions (we will consider this feature in Section 8 in more detail).

We would like to draw readers' attention that the statement about satisfied accuracy of using model of spherical particles (Grenfell & Warren, 1999) in the retrieval of the snow grain size from reflection measurements is completely reasonable when the hemispherical reflectance can be measured. Indeed, it follows from Eq. (1) and from the weak dependence of parameter A on the grain shape, that in this case any microphysical model with equivalent volume-to-surface ratio can be used. But in satellite studies only reflection for the definite positions of the sun and a satellite receiver is available and $R_0(\theta, \theta_0, \varphi)$ in Eq. (13) is a strongly shape-dependent function.

3. Radiance at the top of the atmosphere

To get the radiance at the top of the atmosphere (TOA) measured by a satellite sensor one should take account for the atmosphere–

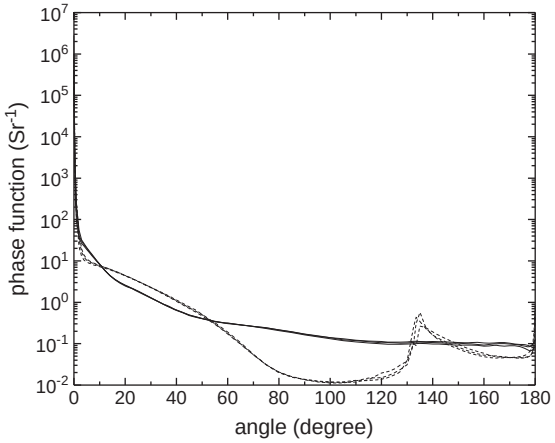

Fig. 1. Phase functions of MIX (solid) and spherical (dashed) grains at wavelengths 469 nm, 858.5 nm, and 1240 nm. Note that the diffraction peak for such large particles is very narrow and value of phase function reaches ~10^6 and more in near forward directions.

snow radiative interaction. In general, the TOA radiance coefficient $R^{TOA}(\theta, \theta_0, \varphi)$ of the system snow–atmosphere is equal to:

$$R^{TOA} = R_{\downarrow}^{Atm} + \sum_{n=0}^{\infty} T_{\uparrow} \otimes \left(R \otimes R_{\uparrow}^{Atm}\right)^n \otimes R \otimes T_{\downarrow}, \tag{14}$$

Here every quantity is a function of the arguments $(\theta, \theta_0, \varphi)$ and sign $\otimes$ denotes the following type of an integral:

$$X \otimes Y = \frac{1}{\pi} \int_0^{2\pi} \int_0^{\pi/2} X(\theta, \theta', \varphi - \varphi') Y(\theta', \theta_0, \varphi') \cos\theta' \sin\theta' d\theta' d\varphi'. \tag{15}$$

In Eq. (14) $R_{\downarrow}^{Atm}$ and $R_{\uparrow}^{Atm}$ are the atmosphere reflectance when illuminated from above and below, respectively; $T_{\downarrow}$ and $T_{\uparrow}$ the transmission functions of the atmosphere when illuminated from above and below, respectively; R is the BRDF of snow; the summation term describes multiple snow–atmosphere reflections; power n denotes the sequence of n integrals.

In what follows we will assume that the atmosphere model is predefined and the reflection and transmission functions of the atmosphere can be computed with the radiative transfer code. Let us introduce the difference of the measured TOA reflectance and the computed reflection function of the atmosphere

$$\Delta R(\theta, \theta_0, \varphi) = R^{TOA}(\theta, \theta_0, \varphi) - R_{\downarrow}^{Atm}(\theta, \theta_0, \varphi). \tag{16}$$

As known, the retrieval of the bi-directional reflection of the underling surface from satellite data (inversion of Eq. (14)) is an extremely complicated problem. That is why the approximation of a Lambertian underlying surface (isotropic BRDF) is often used:

$$R(\theta, \theta_0, \varphi) = r. \tag{17}$$

Within this approximation Eq. (14) becomes the well-known formula:

$$\Delta R(\theta, \theta_0, \varphi) = T(\theta) \frac{r}{1 - r r^{Atm}} T(\theta_0), \tag{18}$$

where $T(\theta)$ is the diffuse transmission coefficient of the atmosphere when illuminated from above by a parallel beam with zenith angle θ:

$$T(\theta) = \frac{1}{\pi} \int_0^{2\pi} \int_0^{\pi/2} T_{\downarrow}^{Atm}(\theta', \theta, \varphi') \cos\theta' \sin\theta' d\theta' d\varphi', \tag{19}$$

r is the surface albedo, r^{Atm} is the atmospheric albedo when illuminated from below:

$$r^{Atm} = \frac{2}{\pi} \int_0^{\pi/2} \int_0^{2\pi} \int_0^{\pi/2} R_{\uparrow}^{Atm}(\theta', \theta, \varphi') \cos\theta' \sin\theta' d\theta' d\varphi' \cos\theta \sin\theta d\theta. \tag{20}$$

However, formula (Eq. (18)) is not accurate enough for the case of snow because of two reasons. First, the BRDF of a snow layer is notably far from isotropic (Nolin & Liang, 2000; Hudson et al., 2006). Second, the atmosphere over snow is often quite clear (especially in polar regions) and contribution of light, reflected by snow layer and transferred through the atmosphere without scattering, is large enough.

To avoid this difficulty the following approximation could be used:

$$\Delta R(\theta, \theta_0, \varphi) = T(\theta) \frac{R(\theta, \theta_0, \varphi)}{1 - r r^{Atm}} T(\theta_0), \tag{21}$$

which partially takes into account the BRDF of the surface. It could be applied to the cases when the angular distribution of the downwelling light transmitted by the atmosphere is much narrower than the surface BRDF. As a case in point, Eq. (21) provides good accuracy for the IR region. However, it is not valid for the cases when a notable part of transmitted light is caused by molecular scattering, e.g., for a short-wave visible region. In this case Eq. (18) is more suitable.

In order to get an approximation valid in both visible and IR regions, we assume that the surface reflection of the direct light transmitted by the atmosphere and the light scattered in the atmosphere near the forward direction is described by the BRDF itself; the reflection of diffusely transmitted light or light multiply reflected in the snow–atmosphere system can be considered as Lambertian (approximation (Eq. (17)). In this regard, we consider the atmospheric transmission as a sum of quasi-direct and diffuse light:

$$\begin{aligned} T_{\downarrow} &= t + T_{\downarrow}^{d}, \\ T_{\uparrow} &= t + T_{\uparrow}^{d}, \end{aligned} \tag{22}$$

where t is quasi-direct transmission:

$$t(\theta, \theta_0, \varphi) = \exp\left(-\frac{\tau^d}{\cos\theta_0}\right) \frac{\delta(\theta - \theta_0)\delta(\varphi - \varphi_0)}{\cos\theta_0 \sin\theta_0}, \tag{23}$$

$\delta(x)$ is the Dirac delta-function, τ^d is the diffusive optical thickness of the atmosphere:

$$\tau^d = \tau(1 - F), \tag{24}$$

τ, the total optical thickness of the atmosphere, F, the part of light scattered into near forward directions.

The assumption that the light multiply reflected in the snow–atmosphere system can be considered as isotropic means that assumption (Eq. (17)) can be applied to terms with $n \geq 1$ in Eq. (14):

$$\begin{aligned} \Delta R(\theta, \theta_0, \varphi) &= T_{\uparrow} \otimes R \otimes T_{\downarrow} + \sum_{n=1}^{\infty} T_{\uparrow} \otimes \left(r \otimes R_{\uparrow}^{Atm}\right)^n \otimes r \otimes T_{\downarrow} \\ &= T_{\uparrow} \otimes R \otimes T_{\downarrow} + T(\theta) \frac{r^2 r^{Atm}}{1 - r r^{Atm}} T(\theta_0). \end{aligned} \tag{25}$$

Putting Eq.(22) into the first term of Eq. (25) we get:

$$\begin{aligned} T_{\uparrow} \otimes R \otimes T_{\downarrow} &= \left(t + T_{\uparrow}^{d}\right) \otimes R \otimes \left(t + T_{\downarrow}^{d}\right) \\ &= t \otimes R \otimes t + T_{\uparrow}^{d} \otimes R \otimes t + t \otimes R \otimes T_{\downarrow}^{d} + T_{\uparrow}^{d} \otimes R \otimes T_{\downarrow}^{d} \end{aligned}. \tag{26}$$

The assumption that the BRDF for diffusely transmitted light can be considered as isotropic means that assumption (Eq. (17)) can be applied to terms with T^d:

$$\begin{aligned} T_{\uparrow} \otimes R \otimes T_{\downarrow} &= t \otimes R \otimes t + T_{\uparrow}^{d} \otimes r \otimes t + t \otimes r \otimes T_{\downarrow}^{d} + T_{\uparrow}^{d} \otimes r \otimes T_{\downarrow}^{d} \\ &= t \otimes (R - r) \otimes t + T_{\uparrow} \otimes r \otimes T_{\downarrow} \\ &= t(\theta)(R(\theta, \theta_0, \varphi) - r) t(\theta_0) + T(\theta) r T(\theta_0) \end{aligned} \tag{27}$$

where

$$t(\theta) = \exp\left(-\frac{\tau^d}{\cos\theta}\right). \tag{28}$$

Putting Eq.(27) into Eq. (25), we finally get:

$$\Delta R(\theta, \theta_0, \varphi) = t(\theta)(R(\theta, \theta_0, \varphi) - r) t(\theta_0) + T(\theta) \frac{r}{1 - r r^{Atm}} T(\theta_0). \tag{29}$$

Eq. (29) partially takes into account the angular features of the snow BRDF through the first term and reduces to the formula (Eq. (18)) for the case of the Lambertian surface.

4. SRS software

We have developed a new software tool SRS (Snow Remote Sensing), specifically to study the accuracy of various analytical approaches and retrieval techniques for snow remote sensing. SRS simulates the bi-directional reflectance from a snow–atmosphere system and the signals in the spectral channels of optical satellite instruments. SRS includes the accurate and fast radiative transfer code RAY (Chaikovskaya et al., 1999; Tynes et al., 2001), realistic changeable atmosphere models with stratification of all components (aerosol, gasses) and realistic models of stratified snow.

The RAY code is intended to calculate radiance and polarization of radiation in the UV, visible, and IR spectral ranges in the system of atmosphere — underlying surface with bi-directional reflectivity. It has been applied with success for the solution of many problems. Validation of the RAY code has demonstrated that it provides highly accurate data in a fraction of time required by the Monte-Carlo and other methods (Tynes et al., 2001; Kokhanovsky et al., 2010). The speed and accuracy of the RAY computations make this code a practical technique for nearly real-time simulations and processing of spectral satellite data.

The input of the atmosphere model includes temperature and pressure profiles, profiles of gas concentration and stratification of aerosol microstructure and concentration. Vertical variations in the snow can be represented in SRS as a collection of homogeneous sub-layers. Each snow sub-layer may contain snow grains with different shapes and sizes and different soot concentrations. The optical properties of snow grains were computed with a Mie code for spherical grains and with the codes (Macke et al., 1996a,b and Yang & Liou, 1996) for non-spherical particles with both ideal and rough surfaces (Shcherbakov et al., 2006) and bubble inclusions. The complex refractive index of ice was taken from the recent measurements of Warren and Brandt (2008). A database of phase functions and single scattering albedo for grains of various shapes for wavelengths, corresponding to MODIS channels 1–6 and 8 was developed and incorporated in SRS.

Here we use the SRS results as a reference to assess the performance of our approximations.

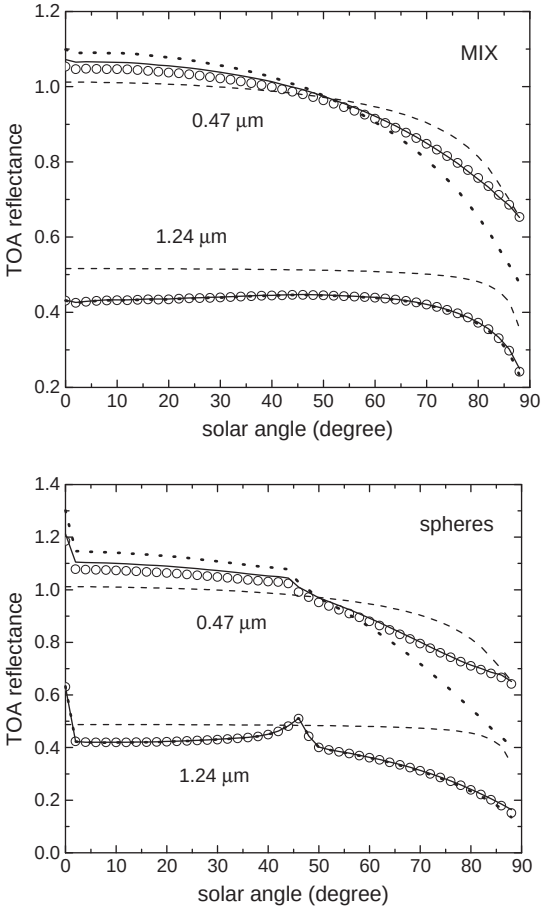

Fig. 2. Reflectance of snow–atmosphere system in MODIS channels 3 (0.47 μm) and 5 (1.24 μm) vs solar angle at nadir observation. Comparison of computations with different approaches: the SRS code (circles), Eq. (29) (solid curves), Lambertian approximation (Eq. (18)) (dashes), and approximation (Eq. (21)) (dots). The Mix model (upper plot), spherical grains (lower plot).

5. Verification of the analytical approach with computer simulation

Earlier we confirmed with SRS the accuracy of the asymptotic formula (Eq. (13)) that is the base of the snow retrieval algorithm (Zege et al., 2008). In this study with focus on the atmospheric correction procedure we will start with verifying Eq. (29). Fig. 2 presents the comparison of three analytical formulas to calculate the TOA reflectance: the approximation of the Lambertian surface (Eq. (18)), the approximation (Eq. (21)) that partially accounts for the bi-directional features of snow reflection, and our approximating formula (Eq. (29)). First, we used the SRS to calculate the atmosphere reflection and transmission functions, the BRDF of snow, and the TOA reflectance. Then we calculated the TOA reflectance by formulas (Eqs. (18), (21), and (29)). We considered two models of snow: spherical grains and the MIX model. Computations were performed for grain effective size of 100 μm. The atmosphere state is characterized by the Background Arctic aerosol (Tomasi et al., 2007) (the minimal amount of aerosol, observed in Arctic) and the Subarctic Winter model of molecular atmosphere, describing the Rayleigh scattering and gas absorption (Kneizys et al., 1996). Simulations were made at two wavelengths, corresponding to MODIS channels 3 and 5 (469 nm and 1240 nm), one in the visible, where the atmosphere–snow interaction is important, and the other in the IR, where molecular and aerosol scattering decrease. It is seen from Fig. 2 that formula (Eq. (29)) has good accuracy in the complete spectral range of interest, both in the short-wave visible, where the contribution of the diffuse light is essential, and in the near IR, where the direct light governs the atmosphere transmission. The Lambertian approximation (Eq. (18)) produces great errors in the IR, where the atmosphere is quite clear and the snow BRDF is significantly far from isotropic (Hudson et al., 2006). The more accurate approximation (Eq. (21)), although being correct in the IR, underestimates the TOA reflectance in visible at the oblique solar angles to 10%. Such an underestimation, although it could be acceptable in some cases of the direct problem, can result in catastrophic errors in the inversions (see Section 8).

6. SGSP algorithm

Putting Eqs. (1) and (13) into Eq. (29), we get the equation that expresses directly the TOA reflection function through the snow characteristics:

$$\Delta R(\theta,\theta_0,\varphi) = t(\theta)\left(R_0(\theta,\theta_0,\varphi)\exp\left[-y\frac{g(\theta)g(\theta_0)}{R_0(\theta,\theta_0,\varphi)}\right]-\exp(-y)\right)t(\theta_0) + \frac{T(\theta)T(\theta_0)}{\exp(y)-r^{Atm}}. \quad (30)$$

We will omit the arguments θ, θ_0, and φ in what follows:

$$\Delta R = \left(R_0\exp\left[-\frac{y}{R_0 G}\right]-\exp(-y)\right)t + \frac{T}{\exp(y)-r^{Atm}}, \quad (31)$$

where

$$\mathrm{t} = t(\theta)t(\theta_0), \quad \mathrm{T} = T(\theta)T(\theta_0), \quad \mathrm{G} = \frac{1}{\mathrm{g}(\theta)\mathrm{g}(\theta_0)}, \tag{32}$$

y is defined by Eq. (11).

As the phase function, and, therefore, the BRDF of a non-absorbing layer, are spectrally constant we can exclude the unknown value R_0 from Eq. (31) by using an additional channel. The use of reflectance in three different channels provides three equations for three independent variables R_0, a_{ef}, and C_{st}*:

$$\Delta R_i = \left(R_0\ exp\left[-\frac{y_i}{R_0\mathrm{G}}\right] - exp(-y_i)\right)\mathrm{t}_i + \frac{\mathrm{T}_i}{\exp(y_i) - r_i^{Atm}}, \tag{33}$$

where i is the channel number.

Note, that this exclusion is one of the key points of this particular algorithm: the use of the extra-channel allows one to avoid any a priori assumption on the snow BRDF that is necessary in all other approaches and may lead to uncontrolled errors of the retrieval.

In our algorithm we use the MODIS channels 3, 2, and 5, as the soot mainly shows itself in the visible (channel 3, 469 nm), whereas the snow absorption appears in the near IR (channel 5, 1240 nm). Channel 2 (858.5 nm) is the additional third channel, where both the snow and the soot absorption are significant. Moreover, none of these channels matches the ozone absorption band.

The system (Eq. (33)) is non-linear, so the solution is found by an iteration scheme. The starting values are found by the least squares method in the assumption that the snow BRDF is isotropic:

$$\begin{aligned}
&R_0^0 = 1,\ a_{ef}^0 = X_1,\ C_{st}^0 = X_2 / X_1,\\
&\begin{pmatrix} X_1 \\ X_2 \end{pmatrix} = \left(\tilde{P} * P\right)^{-1} * \tilde{P} * \begin{pmatrix} Y_3 \\ Y_2 \\ Y_5 \end{pmatrix},\\
&Y_i = \left[\frac{1}{5.8}\ log\left(r_i^{Atm} + \mathrm{T}_i / \Delta R_i\right)\right]^2,\\
&P = 4\pi \begin{pmatrix} \frac{\chi_3}{\lambda_3} & \frac{0.2}{\lambda_3} \\ \frac{\chi_2}{\lambda_2} & \frac{0.2}{\lambda_2} \\ \frac{\chi_5}{\lambda_5} & \frac{0.2}{\lambda_5} \end{pmatrix},
\end{aligned} \tag{34}$$

where λ_i is the wavelength of the ith channel center, χ_i is the imaginary part of the refractive index of ice at λ_i, sign $\tilde{}$ means matrix transposition, * is matrix multiplication.

Then the iterations are performed by the following scheme:

$$\begin{aligned}
R_0^{k+1} &= R_0^k \exp(dX_1),\\
a_{ef}^{k+1} &= a_{ef}^k \exp(dX_2),\\
C_{st}^{k+1} &= C_{st}^k \exp(dX_3),
\end{aligned} \tag{35}$$

where

$$dX = \left(\Delta R - \Delta R^k\right) M^{-1}, \tag{36}$$

$\Delta R = (\Delta R_3, \Delta R_2, \Delta R_5)$ is a vector of radiances measured by MODIS in channels 3, 2, 5; ΔR^k is a vector, calculated by Eq. (33) at the kth iteration step; M is the matrix of derivatives of $\Delta\mathbf{R}^k$ with respect to $\log R_0^k$, $\log a_{ef}^k$, and $\log C_{st}^k$:

$$M = \begin{pmatrix} \frac{\partial \Delta R_3^k}{\partial\ logR_0^k} & \frac{\partial \Delta R_2^k}{\partial\ logR_0^k} & \frac{\partial \Delta R_5^k}{\partial\ logR_0^k} \\ \frac{\partial \Delta R_3^k}{\partial\ loga_{ef}^k} & \frac{\partial \Delta R_2^k}{\partial\ loga_{ef}^k} & \frac{\partial \Delta R_5^k}{\partial\ loga_{ef}^k} \\ \frac{\partial \Delta R_3^k}{\partial\ logC_{st}^k} & \frac{\partial \Delta R_2^k}{\partial\ logC_{st}^k} & \frac{\partial \Delta R_5^k}{\partial\ logC_{st}^k} \end{pmatrix}, \tag{37}$$

where

$$\begin{aligned}
&\frac{\partial \Delta R_i^k}{\partial\ log} R_0^k = \mathrm{t}_i \exp\left(-\frac{y_i^k}{R_0^k \mathrm{G}}\right)\left(R_0^k + \frac{y_i^k}{\mathrm{G}}\right),\\
&\frac{\partial \Delta R_i^k}{\partial\ log} a_{ef}^k = \frac{y_i^k}{2}\frac{\partial \Delta R_i^k}{\partial y_i^k},\\
&\frac{\partial \Delta R_i^k}{\partial\ log} C_{st}^k = \frac{0.2 C_{st}^k}{2}\sqrt{\frac{4\pi a_{ef}^k}{\lambda_i(\chi_i + 0.2 C_{st}^k)}}\frac{\partial \Delta R_i^k}{\partial y_i^k},\\
&\frac{\partial \Delta R_i^k}{\partial y_i^k} = \left(-\frac{1}{\mathrm{G}}\exp\left(-\frac{y_i^k}{R_0^k \mathrm{G}}\right) + \exp\left(-y_i^k\right)\right)\mathrm{t}_i\\
&\qquad - \frac{\exp\left(y_i^k\right)\mathrm{T}_i}{\left(\exp(y_i^k) - r_i^{Atm}\right)^2}.
\end{aligned} \tag{38}$$

The iteration loop breaks when

$$max(\mathbf{dX}) < 10^{-3}. \tag{39}$$

Usually 5 or 6 iterations are needed to converge. If convergence is not reached, the starting values are used as the output.

7. Flowchart and description of the algorithm

Fig. 3 presents the flowchart of the SGSP algorithm. The retrieval algorithm consists of several steps for each pixel. They are:

1. Preliminary separation of the snow pixels. One possibility to get a snow mask is to use the MODIS Snow Cover (MOD10) Level-3 product. This product contains Global snow cover (including snow over ice on large, inland water bodies) mapped daily and as 8-day composites over the Earth's land surfaces at 500 m resolution using the SNOWMAP algorithm (Hall et al., 1995, Klein et al., 1998).
   The other possibility is separating the snow pixels using MODIS Level-1B data. As in the SNOWMAP algorithm, the Normalized Difference Snow Index (*NDSI*) is used for separating of snow pixels (Klein et al., 1998). The input data are the spectral radiance coefficientsR_2, R_4 and R_6, from the MODIS channels 2, 4 and 6 respectively. Every pixel is examined by criteria to be a snow pixel, using the channels 4 and 6. The *NDSI* is computed as

$$NDSI = \frac{R_4 - R_6}{R_4 + R_6}. \tag{40}$$

   A pixel will be mapped as snow if

$$\begin{aligned}
&NDSI \geq 0.4,\\
&R_2 > 0.11,\\
&R_4 \geq 0.1.
\end{aligned} \tag{41}$$

   The criteria (Eq. (41)) provide discarding cloud pixels and efficiently separate snow pixels from water and vegetation ones. It should be noted that separating snow pixels from sea ice pixels

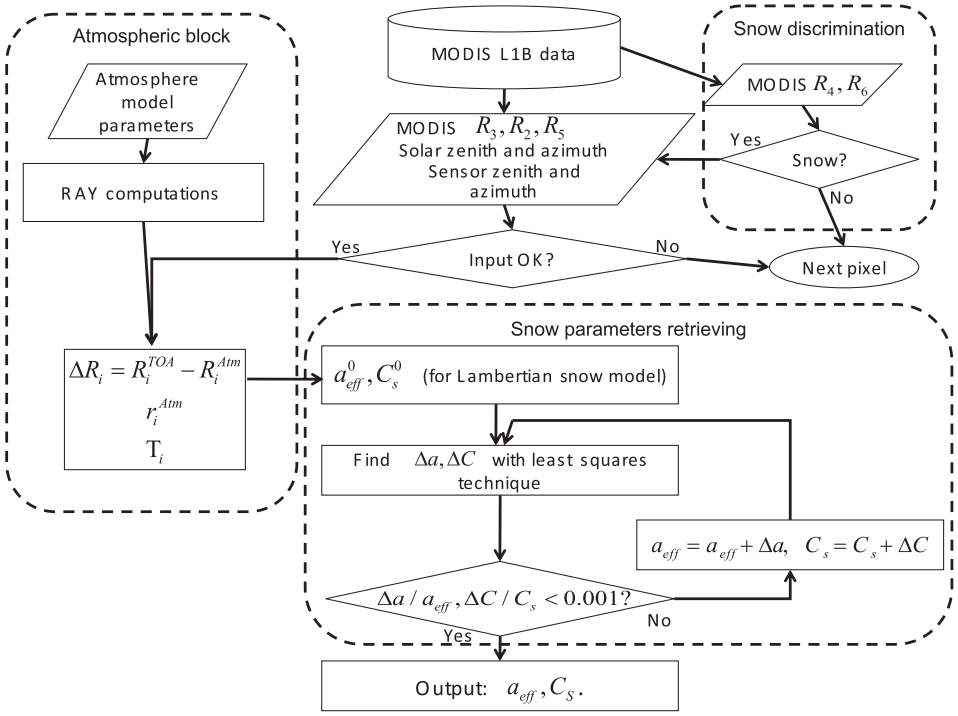

Fig. 3. Flowchart of the SGSP algorithm.

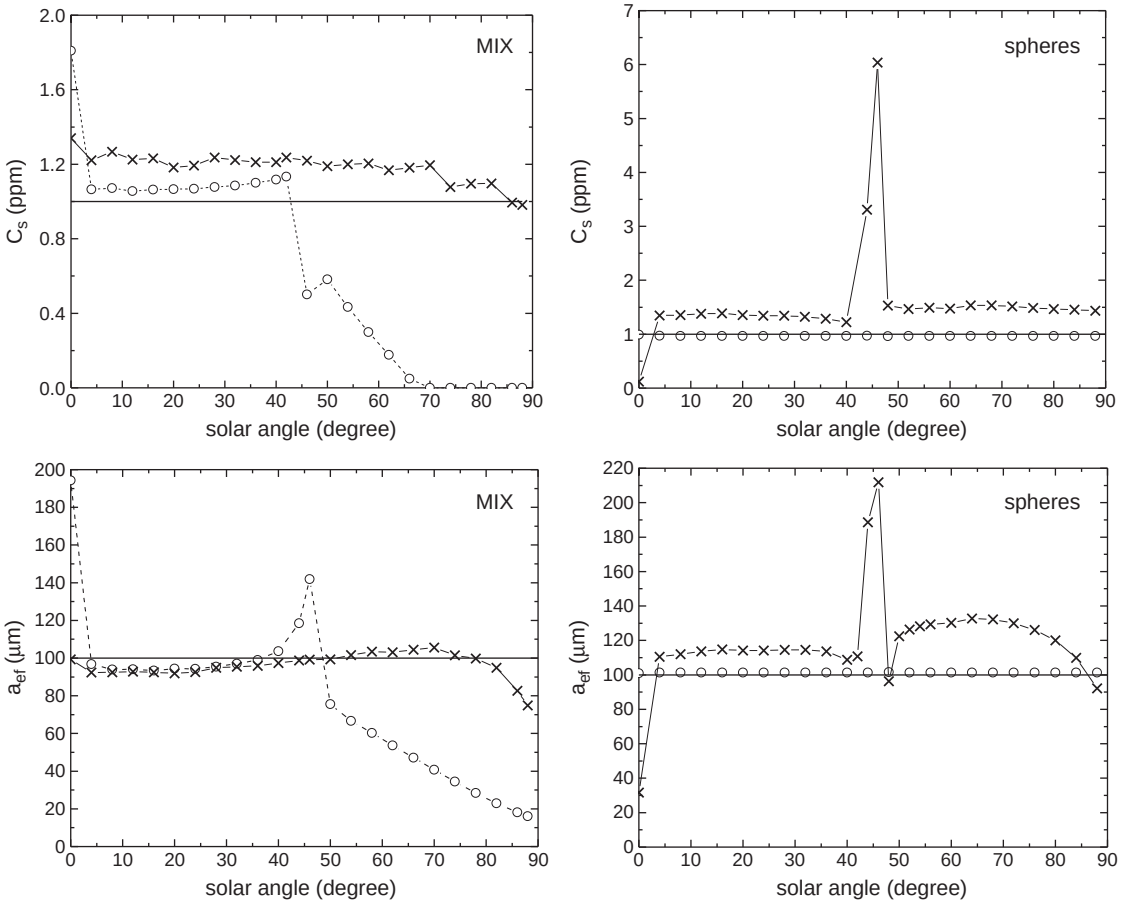

Fig. 4. Retrieval of effective snow grain size and soot concentration by two methods: SGSP (−x) and LUT-Mie (-o) when snow grains are described by MIX model and for snow consisting of spherical grains. Nadir observation. Horizontal lines mark true values.

and discarding pixels with cloud shadow, mixed snow–water, and snow–vegetation pixels require special further attention and development.

Pixels that do not satisfy the criteria (Eq. (41)) are discarded.

2. If the pixel is classified as snow, the radiance coefficients at channels 3, 2 and 5, as well as the solar and observation angles (zenith and azimuth), are read.
3. The atmospheric characteristics $R_{\downarrow}^{Atm}(\theta, \theta_0, \varphi)$, t_i, and T_i are computed with the RAY code. If there is additional information about atmosphere conditions (such as field measurements), any adjusted atmospheric model (thermodynamic or aerosol) can be embedded into the algorithm. If there is no information, we recommend using the Subarctic Winter (Kneizys et al., 1996) and Arctic Background aerosol (Tomasi et al., 2007) models.
4. Finally, the core step is the retrieval of snow grain size and snow impurity concentration from MODIS data.

   The effective size a_{ef} and the soot concentration C_{st}^* are found by the iterative procedure described above (Section 6):

   a. The starting values are found within the approximation of the Lambertian BRDF by Eq. (34).
   b. The iterations are made by Eqs. (35)–(38) until condition (Eq. (39)) is met.
   c. If the iterations have converged, the retrieved values of the effective size a_{ef} and the soot concentration C_{st}^* are the output data; else the output data are the starting values, received at step (a).

8. SGSP algorithm verification

To verify our algorithm we made a closed computer simulation experiment. We specify snow characteristics (soot concentration, grain shapes and sizes) and simulate the spectral radiances at the input of the satellite sensor (MODIS) with the SRS software. Then we use these simulated "MODIS data" as the input for the SGSP algorithm and compare the retrieved and initial data for snow grain size and soot concentration. First, we made calculations without the presence of any atmosphere, in order to show the intrinsic accuracy of the SGSP algorithm. Besides, we applied the algorithm that uses a look-up-table (LUT) based on Mie calculations (Li et al., 2001; Stamnes et al., 2007) to the simulated "MODIS data" and compared results of these two retrievals. The simulation results are presented in Fig. 4. Two cases are considered: the MIX model and the spherical particles. In both cases the effective size is 100 μm and the soot concentration is 1 ppm. It is seen that both methods show good retrieval and close results at high solar angles (from 0° to about 45°). However, the SGSP method provides reasonable accuracy independently of snow grain shapes (both for spheres and the MIX) at all possible solar angles, except for the very narrow rainbow range (about 45°) for spheres. Vice versa, the LUT-Mie retrieval technique that obviously provides excellent accuracy in the case of spherical particles fails when snow grains are not spherical at oblique solar angles. This conclusion is of great importance for snow satellite sensing in polar regions where the sun elevation is low in most cases.

Fig. 5 demonstrates the retrieval accuracy for different grain sizes and soot concentrations. Soot concentrations are retrieved for the effective size of 100 μm (top plot); the effective sizes are retrieved for the soot concentration of 1 ppm (bottom plot). The relative error of the soot concentration retrieval decreases when the soot pollutions increase. It is a few percent for 10 ppm and about 10% for 1 ppm. For lower concentrations the error increases, reaching more than 50% for 0.1 ppm. For pure snow (0 ppm) the retrieved value is about 0.03 ppm. This means that soot concentrations less than 0.05 ppm are practically impossible to sense from reflection. For values about 0.1 ppm it is possible only to estimate the soot concentration by the order of magnitude. A more or less trustworthy retrieval is possible for

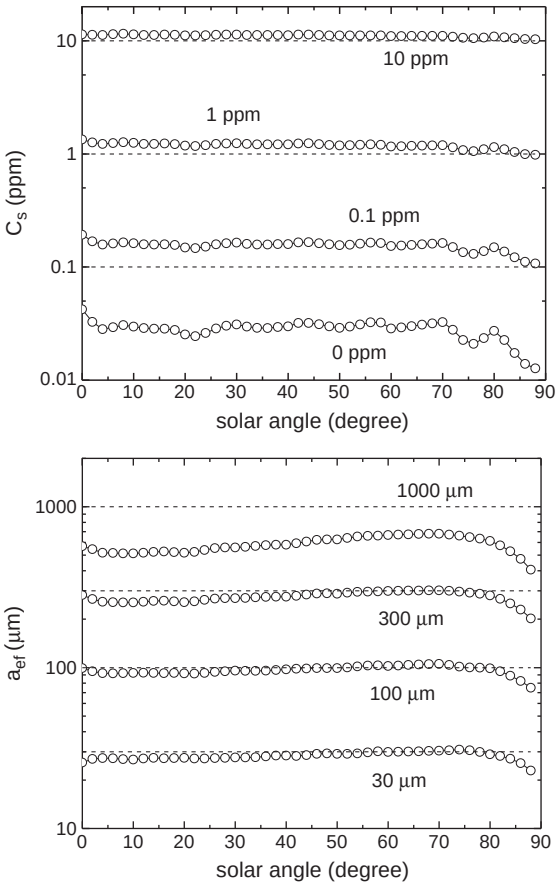

Fig. 5. Retrieval of the snow parameters for different grain sizes and soot concentrations. Retrieved values — o, true values — dashed lines. Grain size is 100 μm in the upper plot; soot concentration is 1 ppm in the lower plot.

concentrations of about 1 ppm and greater. We should note here that this is not a feature of the SGSP algorithm: this follows from the fact that the soot influence on the snow reflection is weak, if its concentration is less than 1 ppm, and is negligible, if its concentration is less than 0.1 ppm.

We see the inverse behavior for size retrieval. The error is a few percent for small particles and increases with size growth. The maximum errors (about 40%) are observed for the largest particles (1000 μm). The reason of this feature is the loss of the accuracy of the asymptotic formula (Eq. (13)) for strong absorption in large snow grain at 1.24 μm (MODIS channel 5) (Zege & Kokhanovsky, 1997). This shortcoming could be fixed by using a satellite sensor with channels in the range of 0.9–1.2 μm (particularly, GLI channel 1.05 μm).

The SGSP algorithm requires as input the atmospheric optical characteristics, which are not known a priori. The difficulties of the aerosol retrieval over bright surfaces like snow are well-known; that is why now we will investigate the algorithm stability with respect to the choice of atmosphere model. As we pay special attention to polar regions, we use various Arctic atmosphere models in our simulations. Unless otherwise specified, the atmospheric thermo-dynamical properties correspond to the Subarctic Winter model (Kneizys et al., 1996), which defines the vertical distribution of the atmosphere parameters (pressure, temperature, and gas concentrations). The Arctic aerosol properties are taken from Tomasi et al. (2007), where the basic aerosol models vary from the Background Arctic aerosol (with the optical thickness of 0.013 at 550 nm) to the Asian Dust (with the optical thickness of 0.19 at 550 nm).

In Fig. 6 some simulation results are presented. We consider again the snow layer, consisting of the MIX grains of the effective size of

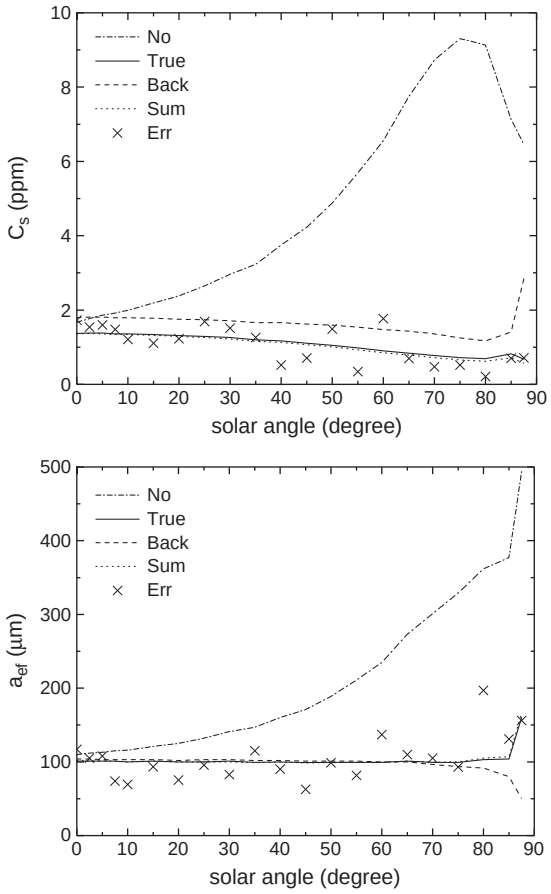

Fig. 6. Sensitivity of the retrieval to the atmosphere models, used in the atmospheric correction procedure (see Table 2 for details).

100 μm, with the relative soot concentration of 1 ppm. The atmospheric aerosol corresponds to the Arctic Haze model (Tomasi et al., 2007) (the optical thickness of 0.13 at 550 nm). The TOA radiances simulated with SRS at MODIS channels 3, 2, and 5 are considered as 'measured signals'. The retrievals are made with different atmosphere models, see Table 2 for details.

The dashed–dotted curve shows the retrieval of the snow layer properties with no atmospheric correction, i.e., as if there is no atmosphere at all. The case demonstrates the necessity of the atmospheric correction because the retrieval is found out to be unsatisfactory, especially at the oblique solar angles.

The other curves demonstrate the algorithm stability with respect to the chosen atmosphere model. Here we retrieve the grain size and the soot concentration under the three following assumptions.

First, the atmospheric properties are considered to be perfectly known. In this example both for simulation of 'measured signals' and in the retrieval process the aerosol is the Arctic Haze; the molecular profile corresponds to the Subarctic Winter model (Kneizys et al., 1996). This case of the retrieval shows the internal errors of the algorithm, which turn out to be not greater than 50% for the soot concentration and a few per cent for the grain size.

Second, the aerosol properties are not known properly (this is the case we usually meet in reality). In this case for the same 'measured signals' as in the previous case (i.e., for the Arctic Haze model) we use the Arctic Background aerosol model in the atmospheric correction. This simulation demonstrates the sensitivity of the retrieval to the aerosol model. It is seen that the soot concentration can be overestimated by a factor of two, which is not catastrophic, whereas the grain size retrieval is weakly sensitive to the aerosol model even at low incidence (sun zenith angles of >75°).

Third, the sensitivity to the molecular profile is checked. The retrieval is made with Subarctic Summer profile instead of the Subarctic Winter. The difference in the retrieval is negligible, what mirrors the stability of the molecular atmosphere in Arctic.

Finally, we investigate the retrieval sensitivity to the measurement error. The random normally-distributed error with the standard deviation of 2%, a value typical for the used MODIS channels and the high radiances of snow, is added to the simulated TOA reflectance. The retrieval was made with the true atmosphere properties, as in the first case.

We can see that the retrieval error is highly sensitive to the measurement error. Moreover, the inaccuracy in the retrieved soot pollution due to the uncertainty in the aerosol model is of the same order as that due to the measurement error of 2%. The inaccuracy of the grain size retrieval due to the uncertainty in the aerosol model is even negligible, as compared to that due to the measurement error. This fact provides two significant conclusions: first, one does not need to know the exact atmosphere aerosol properties and its molecular profile to retrieve the snow layer characteristics, and second, aerosol optical thickness retrieval over snow cover at oblique sun angles with current satellite instruments is hardly possible.

Fig. 7 shows an example of the operational retrieval results without and with the atmospheric correction.

9. Conclusion and discussion

In our previous work we presented the core of the SGSP algorithm to retrieve snow grain size and soot pollution concentration from satellite spectral data (Zege et al., 2008). The strong side of this algorithm is that it does not use any a priori assumptions neither on the shapes of snow particles, or on the BRDF of snow pack. Additionally the analytical retrieval provides extremely fast satellite data processing.

In this paper we have presented a new mature version of the SGSP algorithm enriched by the newly developed atmospheric correction procedure. The verification of the SGSP algorithm using computer simulated signals from an atmosphere–snow system in the spectral channels of the optical satellite instrument has proved that the SGSP retrieval meets accuracy requirements even for polar regions with the low sun position. The verification with field data needs a special attention and such results are going to be published soon.

This operational algorithm is a main result of this work. The SGSP code is realized as Win32 and LINUX console applications. The developed algorithm has been implemented in the near-real time

Table 2
Atmosphere models used in simulation and retrieval procedures.

	Aerosol model	Molecular profile	Measurement error	Legend in Fig. 6
SRS simulation	Arctic haze	Subarctic winter	No	
Retrieval 1	No aerosols	No atmosphere	0%	-.- No
Retrieval 2	Arctic haze	Subarctic winter	0%	— True
Retrieval 3	Background	Subarctic winter	0%	– Back
Retrieval 4	Arctic haze	Subarctic summer	0%	… Sum
Retrieval 5	Arctic haze	Subarctic winter	2%	x Err

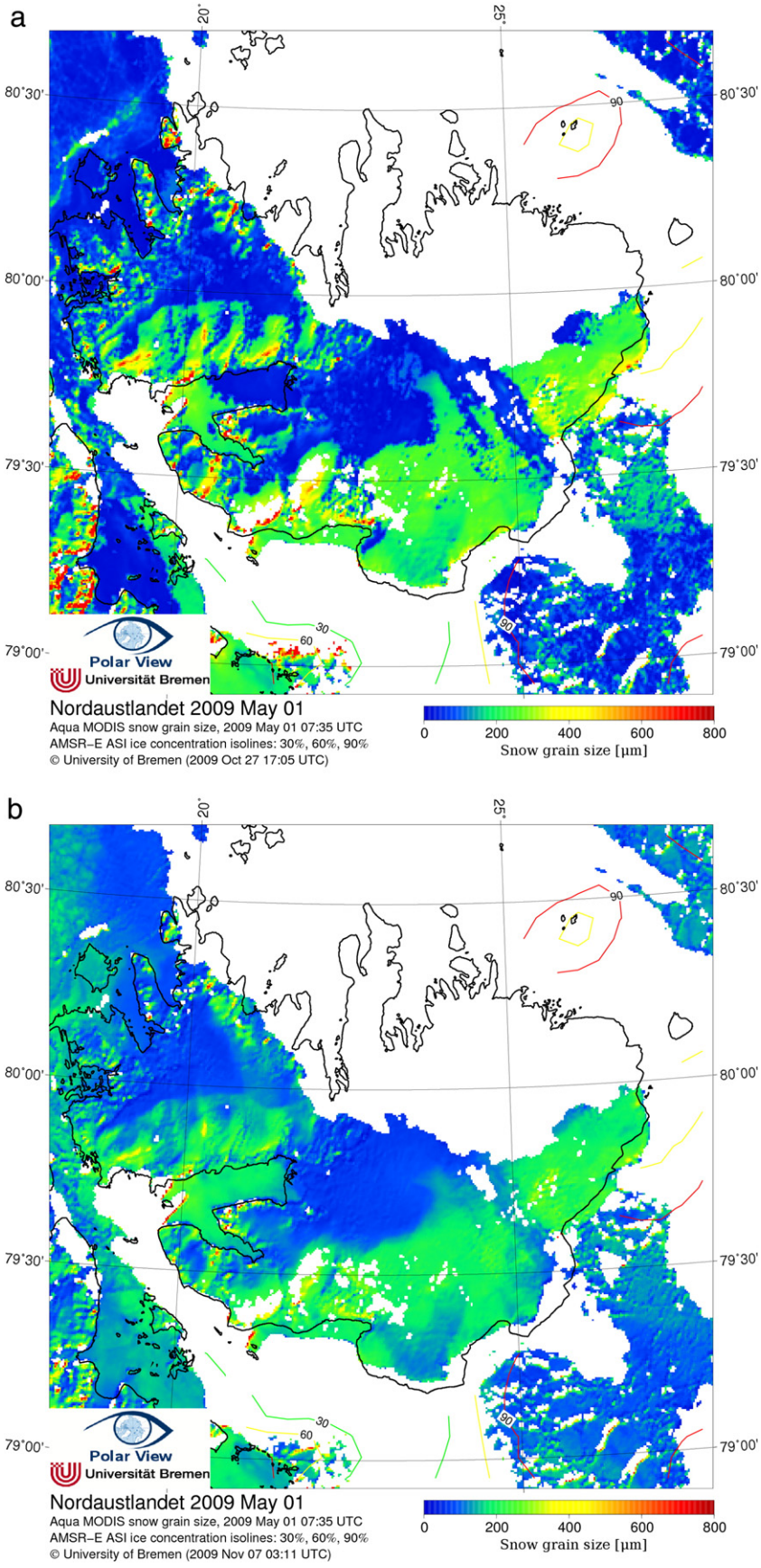

Fig. 7. Retrieval examples as provided in near real time without (upper) and with (lower) atmospheric correction.

MODIS processing chain at the University of Bremen (see http://www.iup.uni-bremen.de:8084/amsr/modis.html), it works operationally and provides the retrieval of the snow characteristics on a regular basis. Retrieved data are available in the online archive http://www.iup.uni-bremen.de:8084/amsredata/modis/.

Besides, we would like to underline the following particular conclusions from performed studies:

1. In polar regions, where the sun position is low, the disregard of the real snow BRDF, particularly, the use of Lambertian reflectance model, as well as the use of the LUT developed with model of spherical particles and Mie code, may lead to unacceptable errors in the retrieved values.
2. The developed iterative atmospheric correction procedure that at least partially allows for the real snow BRDF provides a reasonable accuracy of the snow parameters retrieval even at the low sun positions typical for polar regions.
3. The retrieval error is highly sensitive to the errors of satellite measurements. The inaccuracy in the soot amount retrieval due to the uncertainty in the aerosol model is of the same order as that due to the measurement error of 2%. The inaccuracy of the grain size retrieval due to the uncertainty in the aerosol model is even negligible, as compared to that due to the measurement error. The uncertainty of molecular model of atmosphere practically does not affect the retrieval.

It has been shown more than once (see, e.g., Zege & Kokhanovsky, 1997; Grenfell & Warren, 1999; Gallet et al., 2010), and it obviously follows from Eqs. (1) and (11), that the integral reflectance characteristics, such as albedo or hemispherical reflectance, depend on parameter y only. The weak dependence of parameter A on grain shape allows one to use any microphysical model with equivalent volume-to-surface ratio (e.g., polydispersion of spheres) to describe these integral characteristics. The situation changes in principle when dealing with satellite remote sensing, because the satellite sensors measure only the one value of the BRDF at the particular position of the sun and a satellite receiver. In this case the main shape-dependent factor is $R_0(\theta, \theta_0, \varphi)$, which strongly depends on phase function $p(\theta)$ and, therefore, can differ in orders for oblique incidence (see, Fig. 1, the scattering angles region of about 100°–120°). Removal of this main shape-dependent factor is the point of the SGSP algorithm.

The SGSP retrieval provides a reasonable accuracy for any shapes of snow grains at all possible solar angles. The only exception is the rainbow angle range in the case if snow grains are ideal spheres, what is a very unlikely situation. Vice versa, the method with LUTs based on Mie calculations that obviously provides excellent accuracy for spherical particles, fails for any non-spherical snow grains, that is by far a more realistic scenario, at oblique solar angles. This point makes LUT-Mie retrieval inapplicable for snow satellite remote sensing in polar regions.

Finally, we should note that the retrieved effective grain size is not well-defined microphysical characteristic of snow grains. It is rather an effective optical characteristic, which determines the snow pack reflection. The same concerns the retrieved soot concentration: it may be unknown a priori what substance pollutes the snow, but in this case the equivalent soot concentration that produces the same radiative snow characteristics in the used radiometer channels is retrieved. Strictly speaking, without any assumption and any a priori information we can retrieve only value y from Eq. (11). But it is important that the radiative characteristics of a snow layer depend on this value only, i.e., all the snow microphysical characteristics (size, shape, and pollution) are included into this dependence as one combination — Eq. (11). Therefore, further snow radiative characteristics, such as the spectral albedo, can be retrieved correctly, even if size and pollution are separately retrieved with an error.

As for pollution monitoring, our studies showed that the retrieved soot concentrations are reliable in the range of 1 ppm and greater, in the range of about 100 ppb only the presence of pollution can be detected (with the error of about 50% and more), and no soot can be detected if its concentration in snow is less than 50 ppm. It is worth to mention, though, that the given estimations of the retrieval accuracy consider only the inherent algorithm errors due to the nature of snow reflection. Additional factors (such as surface roughness, field inhomogeneity, stratification, satellite sensor features and so on) should be included in the total realistic error estimations.

Acknowledgments

The authors are thankful to Dr. A. Kokhanovsky for the valuable discussions.

This study was a part of European Integrated Project DAMOCLES. The DAMOCLES project is financed by the European Union in the 6th Framework Programme for Research and Development.

References

Aoki, T., Aoki, T., Fukabori, M., Hachikubo, A., Tachibana, Y., & Nishio, F. (2000). Effects of snow physical parameters on spectral albedo and bi-directional reflectance of snow surface. *Journal of Geophysical Research*, *105* 10 219–10 236.

Aoki, Te., Aoki, Ta., Fukabori, M., Hachikubo, A., & Hori, M. (2003). Effects of snow physical parameters on shortwave broadband albedos. *Journal of Geophysical Research*, *108*, 4616. doi:10.1029/2003JD003506.

Bohren, C. F. (1974). Theory of the optical properties of snow. *Journal of Geophysical Research*, *79*, 4527–4535.

Bohren, C. F., & Huffman, D. R. (1983). *Absorption and scattering of light by small particles.* New York: John Wiley & Sons.

Chaikovskaya, L. I., Katsev, I. L., Prikhach, A. S., & Zege, E. P. (1999). Fast code to compute polarized radiation transfer in the atmosphere–ocean and atmosphere–earth systems. *IGARSS'99, IEEE, International Geoscience and Remote Sensing Symposium, Hamburg, Germany, 1999. Remote Sensing of the System Earth a Challenge for the 21th Century Proceedings-CD-ROM*.

Gallet, J. -C., Domine, F., Zender, C., & Picard, G. (2010). Measurement of the specific surface area of snow using infrared reflectance in an integrating sphere at 1310 and 1550 nm. *The Crysophere*, *3*, 167–182.

Grenfell, T., Warren, S., & Mullen, P. (1994). Reflection of solar radiation by the Antarctic snow surface at ultraviolet, visible, and near-infrared wavelength. *Journal of Geophysical Research*, *99*, 18669–18684.

Grenfell, T., & Warren, S. (1999). Representation of a nonspherical ice particle by a collection of independent spheres for scattering and absorption of radiation. *Journal of Geophysical Research*, *104*(D24), 31697–31709.

Hall, D. K., Riggs, G. A., & Salomonson, V. V (1995). Development of methods for mapping global snow cover using moderate resolution imaging spectroradiometer data. *Remote Sensing of Environment*, *54*, 127–140.

Hori, M., Aoki, T., Stamnes, K., Chen, B., & Li, W. (2001). Preliminary validation of the GLI algorithms with MODIS daytime data. *Polar Meteorology Glaciology*, *15*, 1–20.

Hudson, S. R., Warren, S. G., Brandt, R. E., Grenfell, T. C., & Six, D. (2006). Spectral bidirectional reflectance of Antarctic snow: Measurements and parameterization. *Journal of Geophysical Research*, *111*, D18106. doi:10.1029/2006JD007290.

Kerbrat, M., Pinzer, B., Huthwelker, T., G¨aggeler, H., Ammann, M., & Schneebeli, M. (2008). Measuring the specific surface area of snow with X-ray tomography and gas adsorption: Comparison and implications for surface smoothness. *Atmospheric Chemical Physics*, *8*, 1261–1275.

Klein, A., Hall, D. K., & Riggs, G. A. (1998). Improving snow-cover mapping in forests through the use of a canopy reflectance model. *Hydrological Processes*, *12*(10–11), 1723–1744.

Kneizys, F. X., Robertson, D. C., Abreu, L. W., Acharya, P., Anderson, G. P., Rothman, L. S., et al. (1996). The MODTRAN 2/3 Report and LOWTRAN 7 MODEL. In L. W. Abreu, & G. P. Anderson (Eds.), *Prepared for: Phillips Laboratory, Geophysics Directorate, PL/GPOS, 29 Randolph Road* (pp. 01731–3010). Hanscom AFB: MA.

Kokhanovsky, A. A., & Macke, A. (1997). Integral light scattering and absorption characteristics of large nonspherical particles. *Applied Optics*, *36*, 8785–8790.

Kokhanovsky, A. A., & Zege, E. P. (2004). Scattering optics of snow. *Applied Optics*, *43*(7), 1589–1602.

Kokhanovsky, A. A., Budak, V., Cornet, C., Duan, M., Emde, C., Katsev, I., et al. (2010). Benchmark results in vector atmospheric radiative transfer. *Journal of Quantitative Spectroscopy and Radiative Transfer*, *111*, 1931–1946.

Lenoble, J. (1986). A preliminary cloudless standard atmosphere for radiation computation. *World Climate Programme, World Meteorological Organization*, *112*, 1–40.

Li, W., Stamnes, K., Chen, B., & Xiong, Xiaozhen (2001). Snow grain size retrieved from near-infrared radiances at multiple wavelengths. *Geophysical Research Letters*, *28*, 1699–1702.

Lyapustin, A., Tedesco, M., Wang, Y., Aoki, T., Hori, M., & Kokhanovsky, A. (2009). Retrieval of snow grain size over Greenland from MODIS. *Remote Sensing of Environment*, *113*, 1976–1987.

Macke, A., Mueller, J., & Raschke, E. (1996). Single scattering properties of atmospheric ice crystals. *Journal of Atmospheric Sciences*, *53*, 2813–2825.

Macke, A., Mishchenko, M. I., & Cairns, B. (1996). The influence of inclusions on light scattering by large ice particles. *Journal of Geophysical Research*, *101*(D18), 23311–23316.

Massom, R. A., Eicken, H., Haas, C., Jeffris, M. O., Drinkwater, M. R., Sturm, M., et al. (2001). Snow on Antarctic ice. *Reviews of Geophysics*, *39*, 413–445.

Matzl, M., & Schneebeli, M. (2006). Measuring specific surface area of snow by near-infrared photography. *Journal of Glaciology*, *52*, 558–564.

Nolin, A. W., & Liang, S. (2000). Progress in bi-directional reflectance modeling and applications for surface particulate media: Snow and soils. *Remote Sensing Reviews*, *18*, 307–342.

Picard, G., Arnaud, L., Domine, F., & Fily, M. (2009). Determining snow specific surface area from near-infrared reflectance measurements: Numerical study of the influence of grain shape. *Cold Regions Science and Technology*, *56*, 10–17.

Shcherbakov, V., Gayet, J. -F., Baker, B., & Lawson, P. (2006). Light scattering by single natural ice crystals. *Journal of Atmospheric Sciences*, *63*, 1513–1525.

Stamnes, K., Li, W., Eide, H., Aoki, T., Hori, M., & Storvold, R. (2007). ADEOS-II/GLI snow/ice products — Part I: Scientific basis. *Remote Sensing of the Cryosphere, Special Issue*, *111*(2–3).

Tedesco, M., & Kokhanovsky, A. (2007). The semi-analytical snow retrieval algorithm and 3 its application to MODIS data. *Remote Sensing of Environment*, *111*, 228–241.

Tomasi, C., Vitale, V., Lupi, A., Di Carmine, C., Campanelli, M., Herber, A., et al. (2007). Aerosols in polar regions: A historical overview based on optical depth and in situ observations. *Journal of Geophysical Research*, *112*, D16205. doi:10.1029/2007JD008432.

Tynes, H., Kattawar, G. W., Zege, E. P., Katsev, I. L., Prikhach, A. S., & Chaikovskaya, L. I. (2001). Monte Carlo and multi-component approximation methods for vector radiative transfer by use of effective Mueller matrix calculations. *Applied Optics*, *40*, 400–412.

Warren, S. G., & Brandt, R. E. (2008). Optical constants of ice from the ultraviolet to the microwave: A revised compilation. *Journal of Geophysical Research*, *113*, D14220. doi:10.1029/2007JD009744.

Wiscombe, W. J., & Warren, S. J. (1980a). A model for the spectral albedo of snow. I. Pure snow. *Journal of Atmospheric Sciences*, *37*, 2712–2733.

Wiscombe, W. J., & Warren, S. J. (1980b). A model for the spectral albedo of snow. II. Snow containing atmospheric aerosols. *Journal of Atmospheric Sciences*, *37*, 2734–2745.

Yang, P., & Liou, K. N. (1996). Geometric-optics-integral-equation method for light scattering by nonspherical ice crystals. *Applied Optics*, *35*, 6568–6584.

Zege, E. P., Ivanov, A. P., & Katsev, I. L. (1991). *Image transfer through a scattering medium*. Heidelberg: Springer-Verlag.

Zege, E. P., & Kokhanovsky, A. A. (1997). Approximate formula for the albedo of snow surface. *Izvestiya, Atmospheric and Oceanic Physics*, *33*(5), 667.

Zege, E. P., Kokhanovsky, A. A., Katsev, I. L., Polonsky, I. N., & Prikhach, A. S. (1998). The retrieval of the effective radius of snow grains and control of snow pollution with GLI data. In M. I. Hovenier (Ed.), *Proceedings of conference on light scattering by nonspherical particles: theory, measurements, and applications* (pp. 288–290). Boston, Mass: American Meteorological Society.

Zege, E., Katsev, I., Malinka, A., Prikhach, A., & Polonsky, I. (2008). New algorithm to retrieve the effective snow grain size and pollution amount from satellite data. *Annals of Glaciology*, *49*, 139–144.